Albedo Parametrization for Models of Intermediate Complexity

by

©Sebastian Reyna Martinez

A Dissertation submitted to the Department of Physics and Physical Oceanography
in partial fulfillment of the requirements for the degree of

B.S. Physics (Honours)

Department of Physics and Physical Oceanography

Memorial University of Newfoundland

August 2020

St. John's Newfoundland

Abstract

How much solar radiation a surface absorbs depends on the reflective properties of the specified surface, snow and ice are two surfaces on Earth that have shown to have high albedos due to their reflective properties. To date, albedo schemes are limited to simple parameterizations and to high complexity (also referred to as general circulation) models, the latter being computationally expensive options that require high spatial and temporal resolution, making their usage limited. Models of intermediate complexity (EMICs) aim to be as accurate as general circulation models over similar time scales, and with less computational power. However, for albedo there is as of yet, no appropriate well-tested representation in EMICs. The objective of this thesis was to develop, and test a 'new' parametrization scheme for Earth's seasonal surface albedo; for all terrestrial ice, seasonal snow, and marine ice surfaces. Key variables (wavelength, temperature, snow depth and time) were determined using theoretical schemes and existing data sets were looked at in order to validate the parametrization. However, as data were limited, it was only possible to test a few snow schemes: linear-albedo, linear-albedo for VIS/NIR bands, and polynomial-albedo. It was possible to adjust the polynomial scheme to consider VIS and NIR bands; the results conclude that the polynomial scheme that considers band albedos was the most successful scheme achieved.

Acknowledgements

I wish to thank my supervisor, Dr. Lev Tarasov, for his patience, guidance, feedback and teachings throughout this project. Thanks to Dr. Stephanie Curnoe, for her constant support, help, and advice. I also wish to thank Memorial University of Newfoundland for providing me with this great opportunity to grow. Lastly, I wish to thank my parents and my closest friends for their support throughout this journey.

Table of Contents

Abstract **ii**

Acknowledgments **iii**

List of Figures **vii**

List of Abbreviations and Symbols **ix**

1 Introduction **1**

1.1 Solar Radiation 1

1.2 Albedo 2

1.2.1 The Importance of Albedo 3

1.3 Climate Modelling 3

1.4 Problem 5

1.5 Objective 5

2 Literature Review **6**

2.1 Theoretical Description of Snow and Ice Albedo 6

2.2 Wavelength Dependence 7

2.3 Temperature Dependance 8

2.3.1 Linear Interpolation 9

2.3.2 Polynomial Interpolation 9
2.4 Time Dependance 10
2.4.1 Snow-Ice Transitions 11
2.5 Clouds 12
2.6 Impurities 13
2.7 Solar Zenith Angular Dependance 13
2.8 Spatial Variability 14
2.8.1 Glaciers 14
2.8.2 Snow on forested areas 15
2.9 Data 15
2.9.1 Analyzed Data 15
2.9.2 Characteristic Albedo Values for Different Surfaces 16

3 Parametrization **17**
3.1 Processing Data 17
3.2 Validating Schemes 18
3.2.1 Polynomial Bands 18
3.2.2 Methodology 19
3.2.3 Error Analysis 20

4 Results **21**
4.1 Scheme Error Tables 21
4.1.1 Dye2 and Crawford Point Surface Errors 21
4.1.2 MAR-Greenland Errors 22
4.2 Error Plots 22
4.2.1 Dye2 and Crawford Point Error Plots 23
4.2.2 MAR Data Error Plots 24

4.2.3 MAR Absolute Error Mapping 24

5 Conclusions **26**

References **28**

Appendix A **32**

A.1 Code Description 32

A.2 FERRET Algorithms 38

A.2.1 Mapping the Absolute Error 40

List of Figures

1.1 The Standard Solar Spectrum [NASA, 1974]. 1

2.1 Spectral Reflectance curves [Zeng et al, 1984]. 8

2.2 The major components of the mass budget of a glacier. [Oerlemans, 2010] 14

4.1 MAE for Dye2 23

4.2 RMSE for Dye2 23

4.3 MAE for Crawford Point Surface 23

4.4 RMSE for Crawford Point Surface 23

4.5 MAE for MAR data 24

4.6 RMSE for MAR data 24

4.7 Map for Linear scheme 25

4.8 Map for Linear-bands scheme 25

4.9 Map for Polynomial scheme 25

4.10 Map for Polynomial-bands scheme 25

List of Tables

4.1 Dye2 Surface Errors 21
4.2 Crawford Point Surface Errors 22
4.3 MAR-Greenland Errors 22

List of Abbreviations and Symbols

S_{down}	Total Incoming Radiation.
S_{up}	Total Reflected Radiation.
α	Broadband Albedo.
NOAA	National Oceanic and Atmospheric Administration.
CO2	Carbon Dioxide.
IPCC	The Intergovernmental Panel on Climate Change.
GCM	Global Climate Model.
EMIC	Earth System Model of Intermediate Complexity.
GFDL	Geophysical Fluid Dynamics Laboratory.
NASA	National Aeronautics Space Administration.
UV	Ultraviolet.
VIS	Visible.
IR	InfraRed.
NIR	Near InfraRed.

r_e	Effective Radius
λ	Wavelength.
T	Surface Temperature.
i	Day.
J	Day of Last Snowfall.
τ	Time Scale for Snow-Firn Transitions.
d	Snow Depth.
$d*$	Snow Scale for Snow-Ice Transitions.
A_f	Fractional Forested Area.
A_{nonf}	Fractional NonForested Area.
MAR	Modèle Atmosphérique Régional.
MAE	Mean Absolute Error.
$RMSE$	Root Mean Squared Error.
n	Number of Points.

Chapter 1

Introduction

1.1 Solar Radiation

The sun is known to radiate energy at a wide range of wavelengths (see Figure 1.1), this range is known as the solar spectrum. It can be observed that the magnitude of radiated flux varies with wavelength, and that it radiates at the strongest intensity in the visible range (400 - 750 nm or 0.4 - 0.75 μm); therefore, shortwave radiation is the main focus of this paper, and should be the main focus for albedo schemes, as it is the type of radiation that governs the energy input of the Earth.

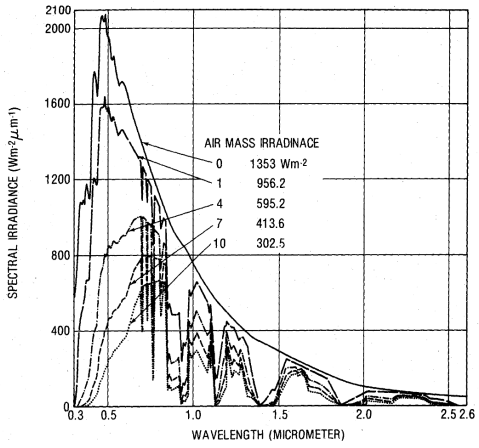

Figure 1.1: The Standard Solar Spectrum [NASA, 1974].

1.2 Albedo

When solar radiation is incident on a surface the laws of optics tell us that a fraction of the incoming radiation will be reflected at the interface of the two media, while the rest of the radiation is absorbed by the surface [Coakley, 1914]. The fraction of reflected radiation at a surface is then dependent on the intensity and spectral (wavelength) distribution of the incident solar radiation, as well as on the reflective properties of the surface in question. The fraction of total reflected radiation is commonly referred to as albedo.

Albedo is a dimensionless quantity that is expressed as the ratio of the total reflected radiation S^{up}, against the total incident radiation S^{down}:

$$\alpha \equiv \int_{sol-spec} \frac{S^{up}}{S^{down}} \quad , \tag{1.1}$$

where the radiative flux ratio is integrated over the entire solar spectrum. Therefore, it is referred to as broadband albedo [Oerlemans, 20010]. If instead, the integration of the ratio is carried over a specific wavelength range (or band), then they are referred to as band or narrow band albedos. Band albedos are of particular interest because the albedo of a surface has different values at different wavelengths, which in turn depend on the surface's reflective properties.

By definition, albedo values are constrained on the interval $0 \leq \alpha \leq 1$. Therefore, high albedo values indicate that the specified surface is reflecting the majority of the total incident radiation, such that as $\alpha \to 1$, all incident radiation is reflected (an ideal reflector), whereas low albedo values indicate that the specified surface is absorbing a large amount of the total incoming radiation, such that as $\alpha \to 0$ all incoming radiation is absorbed (a black body).

1.2.1 The Importance of Albedo

It is known that on average, the albedo at the top of the Earth's atmosphere is about 30% (or 0.3), but varies widely (from about 10% to 90%) across the Earth's surface, and over the seasons (as changes in the physical properties of a surface will impact its reflectivity). Therefore, albedo determines how much radiation is absorbed by the Earth; it then follows that albedo plays a key role in the climate by impacting the energy budget of the Earth directly, which has been noted in several studies (e.g [Kushnir, Y, 2000]).

The energy budget of the Earth strongly impacts snow and ice surfaces, as the recent loss of ice and snow due to Global Warming allows the possibility for positive feedback [NASA, 2009]; therefore, an accurate representation of albedo for these type of surfaces in climate modelling is of importance.

1.3 Climate Modelling

Global climate models (GCMs) are a useful tool for understanding the planet's complex systems, testing theories, and making predictions of the climate over large timescales, among several other applications. The National Oceanic and Atmospheric Administration (NOAA) breaks down the main components of climate models:

- Atmospheric component: simulating clouds, energy and water transfers.
- Land component: simulating vegetation, snow cover, rivers, soil water, as well as CO_2 stored in the soil.
- Ocean component: simulating ocean currents, mixing, and relevant bio-geochemical processes. This component is crucial as the ocean is the largest reservoir (and redistributor) of heat and carbon in the Earth, highlighted on 2019 by the IPPC's

Special Report on Ocean and Cryosphere in a Changing Climate.

- Sea ice component: determining solar radiation absorption and simulating air-sea heat and water transfers.

The NOAA explains that climate models section the Earth into a three-dimensional grid of separate cells, in which each grid cell will represent specific geographic locations and elevations; that is, the Earth is pixelated. For this reason, the term resolution is used is to make reference to the grid size and even time-steps (temporal resolution). In order for grid cells to represent different regions of the planet, there is an associated set of numerical equations to each grid cell; the equations depend on the available input, and on a set of climate variables (i.e. temperature, pressure, moisture, etc). In order to model the components above, it is necessary to model how the grids interact with one another as a coupled system, accounting for matter and energy transfer processes (conservation of energy and momentum). The grid size depends on the computer power available to solve for the numerical equations on each grid cell. Therefore, a finer resolution and a more complex scheme will demand additional computer power in order to perform the simulation, as well as vast internal storage to store and process the simulated data. GCMs aid scientists to determine the degree to which the observed climate changes are driven by natural variability, human activity, or a combination of both [NOAA, no date]. Their data and predictions provide essential information that allows to better inform decision making at national or global levels (e.g. the IPCC reports).

> "Climate modelling at GFDL requires vast computational resources, including supercomputers with thousands of processors and petabytes of data storage." (GFDL, no date)

1.4 Problem

To date, albedo schemes are limited to highly simplistic parameterizations and high complexity options that require a high spatial and temporal resolution. In order for the latter to achieve the desired accuracy and resolution, great computational power is needed, which are very expensive options, thus, making their usage very limited.

Earth system models of intermediate complexity (EMICs) aim to be accurate over long time periods with less computational power. They are the bridge between the simple climate models and the computationally expensive general circulation models. For albedo there is as of yet no appropriate well-tested representation in EMICs.

1.5 Objective

The objective of this thesis is to develop, test, and validate a 'new' parametrization scheme for Earth's seasonal surface albedo for all terrestrial ice, and seasonal snow surfaces. These surfaces are the focus of this thesis as snow and ice albedo have a very strong influence on the climate and on the surface energy balance [Klok and Oerlemans, 2004]. The parametrization scheme should be an adequate scheme for EMIC's.

Chapter 2

Literature Review

2.1 Theoretical Description of Snow and Ice Albedo

The albedo of snow and ice changes constantly throughout the year. Oerlemans explains that fresh snow has the highest albedo values. As time passes, the aging of the snow is related to changes in its crystal structure, that lead to a lowering in albedo. Particularly in summer, further melting and accumulation of impurities at the surface affect its structure, causing further decline [Oerlemans, 2010].

The aging of snow has been discussed in previously developed theoretical schemes for albedo, where the optical theory of the reflective properties of snow and ice is discussed in detail. Highlighting that snow surfaces can be described as a collection of solid water (ice) spheres with the same specific surface area and an effective radius r_e [Gardner and Sharp, 2010]. As reflections occur at the boundary between two different mediums, they summarized snow albedo's behaviour through statistical analysis. A larger spherical grain radius increases the average travel path of the photons within the ice grain, which increases the probability of their absorption. While a smaller radius shortens the travel path, increasing the number of air-ice interfaces, thus, increasing

the probability for a photon to be reflected out of the snowpack. On the other hand, Warren et al. determined that ice albedo is governed by size and distribution of air bubbles, and cracks within the ice. That is because the more air-ice interfaces or the larger the surface area of the interface, the greater the probability for a photon to encounter an interface where they get reflected out. On ice particularly, liquid water greatly reduces shortwave albedo as it increases transmittance by reducing the number of air-ice boundaries that exist near the surface of the ice (ice cracks filled by water) [Warren et al, 2002].

2.2 Wavelength Dependence

The wavelength dependance for snow and ice surfaces at different evolutionary stages (age) has been documented in the characteristic spectral curves for ice, dirty ice, snow and old snow of Zeng et al, in 1984, as well as in Gardner's and Sharp's theoretical albedo parametrization in 2010. Both showing that nearly all radiation with $\lambda > 1.5$ μm is absorbed within the first few millimetres of a the surface. That is, snow and ice are absorptive in the near infrared (NIR: 750-1000 nm) spectrum, but good reflectors in the visible (VIS) spectrum. Particularly, Zeng's study showed that for both snow and ice there is a near constant difference between the VIS-albedos and NIR-albedos [Zeng et al, 1984]. From the spectral curves it can be observed that albedo for firn at VIS wavelengths can match albedo values for snow at NIR wavelengths. As this wavelength dependance, is as strong as the grain size (age) dependance. For an ice surface there is a relatively constant difference between visible and near-IR [Knap et al. 1999]. Wavelength should be then considered as a key variable for modelling snow and ice albedo (see Figure 2.1).

Oerlemans explains that the albedo of pure ice has has been found to drop off faster

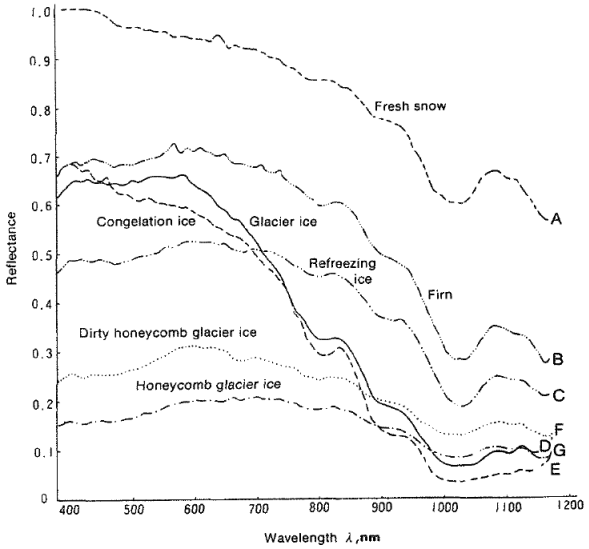

Figure 2.1: Spectral Reflectance curves [Zeng et al, 1984].

(higher sensitivity) than the albedo of snow with increasing wavelength [Oerlemans, 2010]. However, when ice is sufficiently impure (dirty), its spectral dependence is very weak [Zeng et al, 1984]. Therefore, when accounting for dirty ice in an model, it should be considered to be wavelength independent.

2.3 Temperature Dependance

Temperature varies throughout the year, causing snow grains to be melted and re-frozen, becoming 'larger' grains; increasing the probability of photon absorption. On ice, the ice cracks are filled when melting occurs, increasing absorption probability as well. As such, temperature dependance can approximately model snow and ice ages.

There exist several ways to account for the age of snow through temperature, the ones considered are discussed in the subsections bellow.

2.3.1 Linear Interpolation

A particularly direct and efficient method to model the age of ice or snow is the linear interpolation scheme. This approach has been carried out in previous studies (e.g. [Roesch et al, 1999]) and used in several circulation models like ECHAM4,

$$\alpha = \alpha_{max} - (\alpha_{min}) \cdot \frac{T - T_0}{T_m - T_0} \quad , \tag{2.1}$$

where the constants α_{max} ,and α_{min} are the maximum and minimum characteristic albedo values for snow, that is the characteristic value for new snow and the characteristic value for old snow (firn) respectively. While the constants T_0 and T_m define the limits for which this transformation occurs. The most commonly employed range in literature is from T_0 = - 10 °C to the melting temperature of water T_m = 0 °C.

This is a very useful model as it can also model ice albedo by simply setting the maximum and minimum characteristic albedo values to those of pure ice and melting ice respectively, and by adjusting the temperature range. Similarly, it can be modified to model the VIS and NIR bands for both snow and ice, giving four linear equations in total, one each for snowVIS, snowNIR, iceVIS, and iceNIR; through which we can model the broadband (final) albedo for snow and ice using a conversion scheme. This scheme accounts for the strong impacts that wavelengths have on snow and ice albedo as well the temperature dependance. It has has been widely used in the literature (e.g [Collins, 2002]), as well as in climate models such as the NCAR.

2.3.2 Polynomial Interpolation

Another 'simple' scheme is the polynomial interpolation scheme by Roesch (1999),

$$\alpha = 0.5 + (-0.0758627) * T + (-5.5360168E - 3) * T^2 \\ +(-5.2966269E - 5) * T^3 + (4.2372742E - 6) * T^4 \quad , \tag{2.2}$$

where the temperature T must be in units Celsius, and the constants were set such that the scheme was designed to model broadband snow albedo range ($0.8 \geq \alpha \geq 0.5$). With $\alpha = 0.8$ when T $\leq$ -10 °C, and with $\alpha = 0.5$ when T $\geq$ 0 °C. This model has been noted to perform best in comparison to the linear models, for a more detailed description see Køltzow (2007).

2.4 Time Dependance

It is important to highlight that temperature solely does not account adequately for snow evolution. If the temperature decreases, firn will not turn into new snow. That is, temperature variations make snow grains coarser, not finer. Therefore, it is crucial to highlight that there is a time dependance of snow that unrelated to temperature.

A simple albedo parameterization scheme that accounts for the age for snow was developed [Oerlemans, and Knap, 1998]. Using data from the Morteratsch Automatic Weather Station, they focused on the observed albedo exponential 'behaviour' and considered the following variables as their main input parameters: global radiation, snowfall dates, and snow depth. Showing that the albedo for snow can be modelled as:

$$\alpha_{snow}(i) = \alpha_{firn} + (\alpha_{frsno} - \alpha_{firn}) \cdot \exp\Big[\frac{(J-i)}{\tau}\Big] \quad . \tag{2.3}$$

This is a daily model where i indicates the time-step in the numeric equation (1 day in this case). Where J is the day of the last snowfall and τ is the time scale

that determines how fast the albedo of fresh/new snow (frsno) approaches albedo of old snow (firn) after a snowfall. For this model, fresh snow is considered to be up to one day old. As they had no data on snow falls, the snowfall day J was determined through snow depth with the following algorithm:

If $d(i) - d(i-1) \geq 0.02$ m, then $i = J$.

It is clear the key role that snowfalls play by adding new snow, on top of firn, ice or whatever background surface is chosen. Therefore, transitions between snow and other surfaces should be considered.

2.4.1 Snow-Ice Transitions

When there is a snow surface overlapping with an ice surface, if the snow layer is not sufficiently thick it cannot be considered as uniform snow surface that can be associated to a single albedo value. For this reason, Oerlemans and Knap account for snow-ice transitions when the thickness is sufficiently small,

$$\alpha(i) = \alpha_{snow}(i) + [\alpha_{ice} - \alpha_{snow}(i)] \cdot \exp\Big(\frac{-d}{d^*}\Big) \quad , \tag{2.4}$$

where $d^* = 0.03$ m is a characteristic scale for snow depth, and when $d = d^*$ snow contributes 1/e to albedo. The depth 'd' could be taken to be an input parameter from a particular data set or if needed be, a function of snow water equivalent or another climate variable [Oerlemans and Knap, 1998].

When new snow overlays on top of pure white ice (with a 0.4 albedo), if the snow depth is greater than 10mm thick then the snow albedo in the near-UV and visible wavelengths (0.3 - 0.7 μm) is minimally affected, and the albedo in the shortwave IR (0.75 - 1.5 μm) is completely unaffected. While for very coarse snow (with an effective radius 1 mm - 5 mm) the depth must be $>$ 100 mm in order for its albedo to remain

unaffected in the near-UV [Gardner and Sharp, 2010]. Highlighting the importance of age and wavelength dependance

These types of schemes are commonly called empirical, as they reproduce observed behaviours shown by measured data. Oerlemans and Knap developed schemes that consist of making albedo values transition exponentially from the characteristic value of fresh snow (or grains with $r_e = 0.1$ mm) to a representative value of old snow ($r_e =$ 1 mm) or from snow to ice when the there is not enough snow lying on top of an ice surface. Oerlemans explained that ice albedo is time dependant, when pure ice is exposed to the environment, it will lose its purity (becoming dirty ice). Dirty ice depends on the several impurities which can land on or grow beneath the surface over time, such as dust, dirt, carbon, aerosols or algae [Oerlemans, 2010].

Ice albedo's dependance on ice thickness, can be modelled with a linear decrease towards ocean albedo can be applied as thinner ice transitions into ocean surface, for ice whose thickness ≤ 0.25 m [Perovic and Grenfell, 1981]. Koltzow (2007) included this on one of his several parametrization for sea ice; however, the lack of data did not allow further testing and analysis of the model.

2.5 Clouds

Clouds filter out solar radiation with $\lambda > .8$ μm, and based on a set of different observational studies, he determined that multiple reflections between surface and clouds play a key role in albedo, where multiple reflections between the surfaces and the clouds cause a spectral shift towards the visible wavelengths [Oerlemans, 2010]. The broadband albedo for snow and ice increases with cloud optical thickness, as clouds absorb IR and reflect VIS radiation, that is, clouds will reflect back any VIS radiation already reflected by snow or ice [Gardner and Sharp, 2010]. The greater

the clouds optical thickness, the stronger the shift. The stronger the shift, the more radiation is received in the visible spectrum where snow and ice are good reflectors.

2.6 Impurities

For both snow and ice, impurities located near the top of the surface are the ones that have the greatest impact on albedo. The effect of all impurities can be summarized by accounting for externally mixed carbon particles as they are more absorbent than other impurities like dust or ash. These impurities lower snow albedo in the region where absorption by ice is weakest ($\lambda < 0.9$ μm), and causing the greatest reductions in albedo for coarse-grain type snow; on the other hand, for solar radiation with $\lambda > 0.9$ μm, the effect of impurities on snow albedo is negligible since ice has already a strong absorption at these wavelengths [Gardner and Sharp, 2010]. Highlighting that snow and ice containing impurities reduce the spectral shift effect caused by clouds by making the surfaces to be as absorbent as they would be in the Infrared.

This is a relevant role of impurities on snow and ice albedo, as it can greatly reduce the albedo of a surface. A good analogy is the effect of green house gases trapping energy within the atmosphere; while impurities trap energy within the surface, making it prone to melting, causing further albedo lowering (which can cause positive feedbacks). Therefore, it should be considered in models.

2.7 Solar Zenith Angular Dependance

Gardner and Sharp explain that the albedo of snow has been found to increase in the near-IR region with increasing incident angle, as on average a travel path that is closer to the surface is more likely to experience scattering as snow grains are often smaller near the surface. Particularly, near-UV and visible wavelengths experience

such low absorption that albedo remains the same regardless of the incident angle, and that very little energy from the sun is actually received at high zenith angles [Gardner and Sharp, 2010]. This information allows us to discard solar zenith angle as a key variable.

2.8 Spatial Variability

The United States Geological Survey contains data that can be used to determine the land types: forested vs non forested, as well as the fractional snow covered area for the western United States.

2.8.1 Glaciers

In the ablation area, the lateral variations in the albedo are much larger than the altitudinal variations; however higher albedos are expected on the accumulation zone of a glacier, while lower albedos are expected in the ablation area (Oerlemans, 2010, p80). He also mentions that clean glacier ice is generally surrounded by debris-covered ice (dirty ice) with typical value 0.15 .

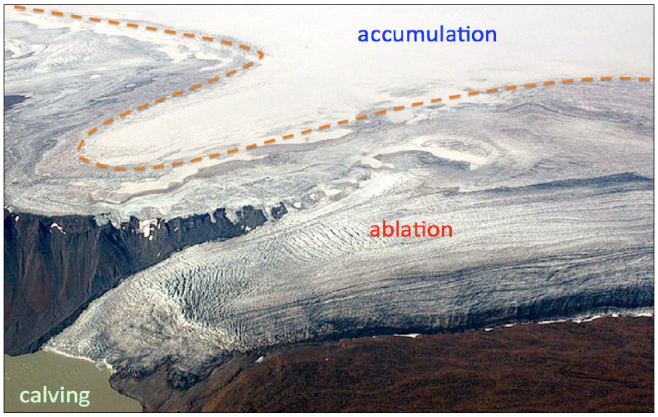

Figure 2.2: The major components of the mass budget of a glacier. [Oerlemans, 2010]

2.8.2 Snow on forested areas

The total snow albedo can be calculated based on the fraction of a grid cell covered by forest (e.g. [Roesch et al, 1999]):

$$\alpha_{snow}(i) = A_f(i) \cdot \alpha_{forest}(i) + A_{nonf}(i) \cdot \alpha_{snow}(i) \tag{2.5}$$

The variable A_f is the fractional area of a grid cell that is covered by forest and and A_{nonf} is the fractional area that is nonforested, that is $A_{nonf}(i) = 1 - A_f(i)$.

2.9 Data

2.9.1 Analyzed Data

All data used for the model was obtained from the Arctic Data Center. An online platform where scientists share, discover, access, and analyze data about the Arctic. Most files uploaded into the platform are NetCDF files. NetCDF files are a set of scientific software libraries and data formats that support the creation, access, and sharing of array-oriented data. Several data sets were looked at. However, only a few sets were found to have a few of the variables that were needed for the model, others did not have the minimum required variables. The chosen data files were:

- NetCDF data: from Dye2 surface in Greenland from Baptiste Vandecrux (2018).
- NetCDF data: from Crawford Point surface in Greenland from Baptiste Vandecrux (2018).
- NetCDF data: from Model simulations from Modèle Atmosphérique Régional (MAR) over Greenland (2016). This data set simulates all of Greenland though a grid with a spatial resolution of 25km.

2.9.2 Characteristic Albedo Values for Different Surfaces

The characteristic albedo values for different surfaces have been documented by several studies. The following values were ones the chosen in order to maintain consistency in the ranges. In both studies Roesch modelled albedo under the common temperature range, from -10 °C to 0 °C.

- New-snow: $\alpha = 0.8$ (Roesch thesis, 1999).
- Old-snow: $\alpha = 0.5$ (Roesch thesis, 1999).
- New-snowVIS: $\alpha = 0.95$ (Roesch et al, 2002).
- New-snowNIR: $\alpha = 0.65$ (Roesch et al, 2002).
- Old-snowVIS: $\alpha = 0.57$ (Roesch et al, 2002).
- Old-snowNIR: $\alpha = 0.39$ (Roesch et al, 2002).

Chapter 3

Parametrization

3.1 Processing Data

Although the data from Crawford Point surface and Dye 2 surface was plentiful, the variables recorded in these two data sets were limited to measured albedo and surface temperature; thus, it was only possible to validate temperature dependent schemes for these sites. On the other hand, the MAR data set includes a wide range of variables, however, the data was difficult to process with C as a segmentation fault would occur; however, this can be avoided by allocating the data on a different memory location instead. FERRET; however, allows for handling, processing and analysis of data, but it is an inadequate software for creating the complex algorithms that can be achieved with a programming language, and that were needed to achieve a more complex scheme. This, along with a lack of input variables on the first two data sets mentioned, it was only possible to model and validate surface albedo, using only the selected temperature schemes.

3.2 Validating Schemes

Based on the set backs detailed in Section 3.1, the selected schemes were those that were dependant on the available key variables: Temperature, Measured Albedo, and time-step. The schemes that were able to coded and validated were:

1. Linear Scheme: See Section 2.3.1
2. Linear-BANDS Scheme: See Section 2.3.1
3. Polynomial Scheme : See Section 2.3.2

Koltzow (2007) compared several albedo schemes, concluding that the polynomial scheme was in better agreement with the observations than the linear schemes. It was also been reported that linear schemes over/under estimate the albedo as they change immediately with temperature. However, as we know from thermodynamics, as solid water (which exists below 0 ^{o}C) intakes energy, its temperature will first increase to 0 ^{o}C degrees before it absorbs the energy required to change states. Since surface transformations are not immediate, a polynomial scheme presents itself to be the best temperature dependent scheme to account for this delay.

From Section 2.2 we highlight the constant difference between visible and near infrared band albedos and the usefulness of the polynomial scheme which accounts for a slower surface transformation, to come up with a 'new' temperature scheme which takes into account these two important features.

3.2.1 Polynomial Bands

Using the polynomial approach to account for non-instantaneous snow transitions, and some adjustments, it was possible to model both VIS and NIR albedo bands. However, the adjustments were not ideal, as the polynomial scheme was designed to

fit particular (broadband snow) values, $0.8 > \alpha > 0.5$ in the surface temperature range -10 °C $< T <$ 0 °C.

The following adjustments were carried out:

- The snow NIR-albedo was obtained by adjusting the minimum value from 0.5 to 0.39, and setting the maximum albedo to 0.65. Whenever, $\alpha_{NIR} > 0.65$ or whenever $T <$ -10 °C.

- The snow VIR-albedo was obtained by adjusting the minimum value from 0.5 to 0.57 and limiting the maximum albedo value to 0.8, when $T <$ -4.25 °C. Such that if $T <$ -4.25 °C, then it evaluates albedo using a linear interpolation in range -10 °C to -4.25 °C, with a max albedo of 0.95 and a minimum of 0.8.

3.2.2 Methodology

The temperature range and max and min values were chosen the same for all schemes: 0.8 and 0.5 respectively. This was in order to have a mode adequate comparison of snow albedo models. Studies in the past like the one from Koltzow, have compared albedo schemes; however, the temperature ranges and the characteristic values are different between them. Therefore, in order to make a more specific testing; the limits and temperature ranges were set to be the same for all. So that solely the efficiency of the schemes is validated, and not the efficiency of the constants, nor that of the ranges.

For Dye2 and Crawford-Point surface data: the C code scans two variables, measured albedo and measured temperature. For each scan it evaluates each of the four temperature schemes discussed above. The output is printed and stored for further error analysis[1].

[1]For a detailed description of the code see subsection Appendix A.1

For MAR's simulated data: FERRET was used instead of C to handle all the data, evaluating the schemes, and storing output for further error analysis. As this data set is gridded, it was possible to map the absolute error of each scheme with FERRET[2].

3.2.3 Error Analysis

Over the last few decades, the mean absolute error (MAE) and the root mean square error (RMSE) have been regularly employed in model assessment studies. There are defined as,

$$MAE = \frac{\Sigma_i^n |\alpha_i - \alpha|}{n} \quad , \tag{3.1}$$

$$RMSE = \sqrt{\frac{\Sigma_i^n (\alpha_i - \alpha)^2}{n}} \quad . \tag{3.2}$$

Researchers have thoroughly discussed and attempted to determine which of these statistical error schemes is best one for assessing a model's performance [3]. As the MAE assigns the same weight to all errors, while the RMSE heavily penalizes larger values. Both errors schemes have been relevant and present in the previous literature; therefore, both the MAE and RMSE were calculated for each snow scheme listed, per each of the data sets described.

[2]For FERRET algorithms and mapping see Appendix A.2
[3]For more information, see Chai (2014) and Willmott (2005)

Chapter 4

Results

The results presented in this chapter are the output from the MAE and RMSE functions . The schemes: Linear, Linear Bands, Polynomial and Polynomial Bands where numbered 1, 2, 3, and 4 respectively.

In the following section, tables with the error output per each data set are presented, listed are: the validated scheme, and both the MAE and the RSME associated with each of them. For a visual guide, see Section 4.2.

4.1 Scheme Error Tables

4.1.1 Dye2 and Crawford Point Surface Errors

Scheme	MAE	RMSE
1	0.123437	0.169442
2	0.124216	0.170984
3	0.110225	0.156080
4	0.112911	0.158831

Table 4.1: Dye2 Surface Errors

Scheme	MAE	RMSE
1	0.125159	0.165500
2	0.125772	0.166902
3	0.110349	0.148941
4	0.113286	0.152141

Table 4.2: Crawford Point Surface Errors

4.1.2 MAR-Greenland Errors

Scheme	MAE	RMSE
1	0.28377	0.40170
2	0.28409	0.40158
3	0.28045	0.40605
4	0.28187	0.40707

Table 4.3: MAR-Greenland Errors

4.2 Error Plots

This section provides a graph for each of the tables presented above, as well as an error map of Greenland for each of the schemes.

4.2.1 Dye2 and Crawford Point Error Plots

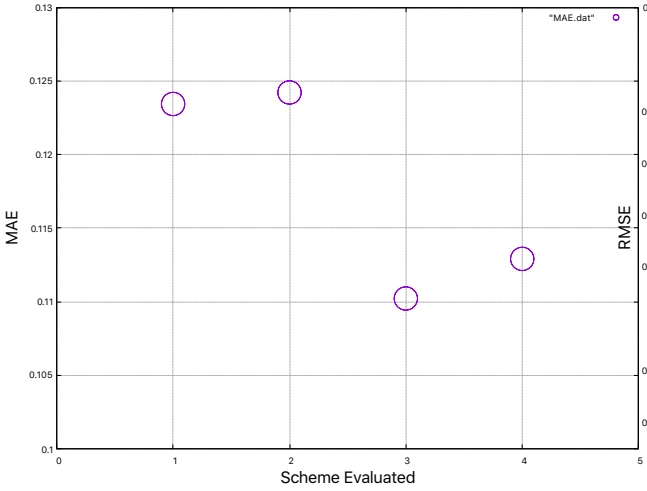

Figure 4.1: MAE for Dye2

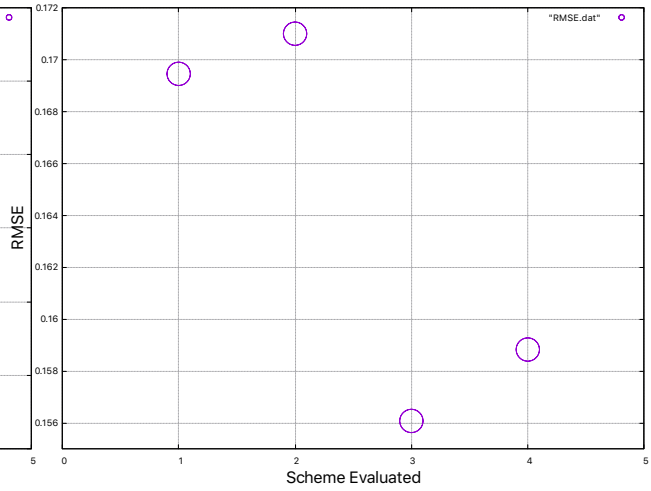

Figure 4.2: RMSE for Dye2

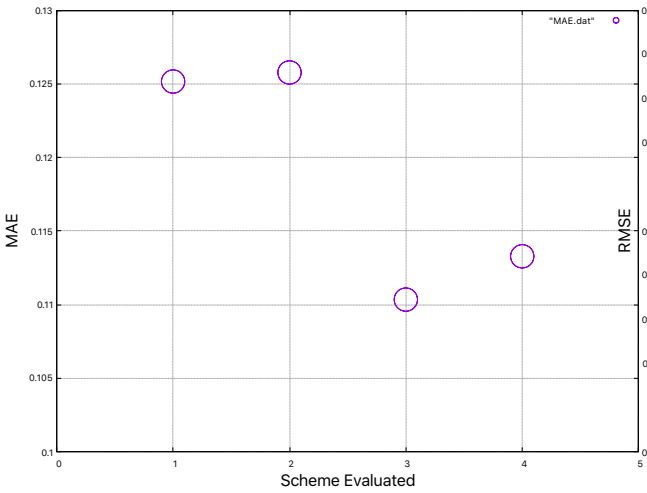

Figure 4.3: MAE for Crawford Point Surface

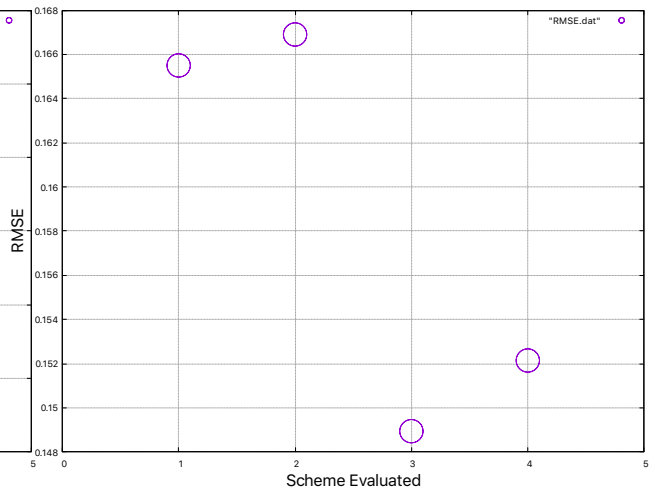

Figure 4.4: RMSE for Crawford Point Surface

4.2.2 MAR Data Error Plots

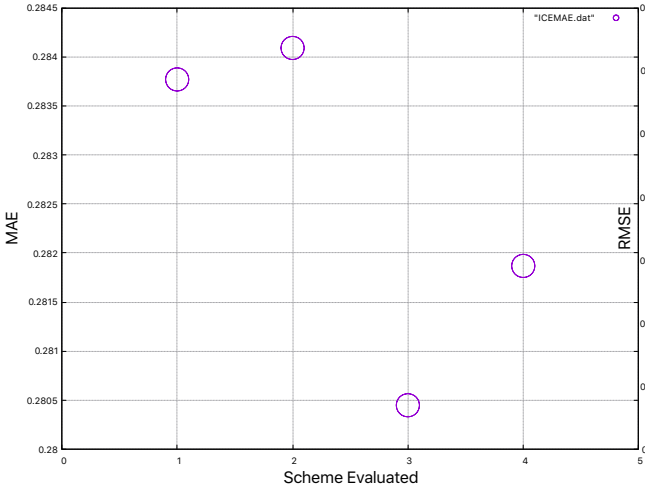

Figure 4.5: MAE for MAR data

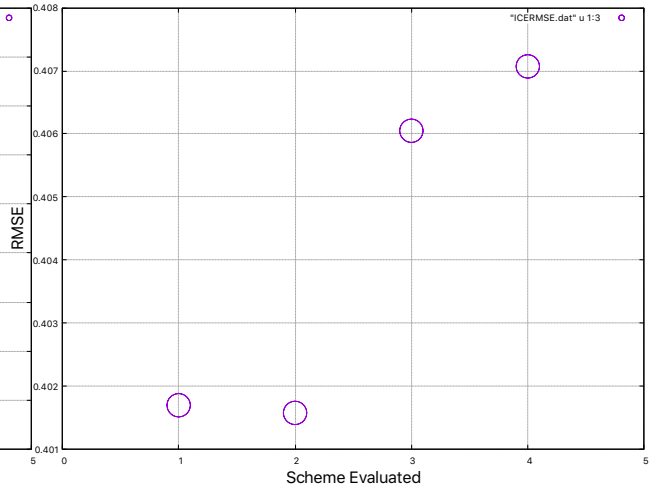

Figure 4.6: RMSE for MAR data

4.2.3 MAR Absolute Error Mapping

This sections shows the FERRET absolute error mappings that were obtained for each scheme. Showing that the polynomial-band scheme is the scheme which covered the largest extent of area with the least error.

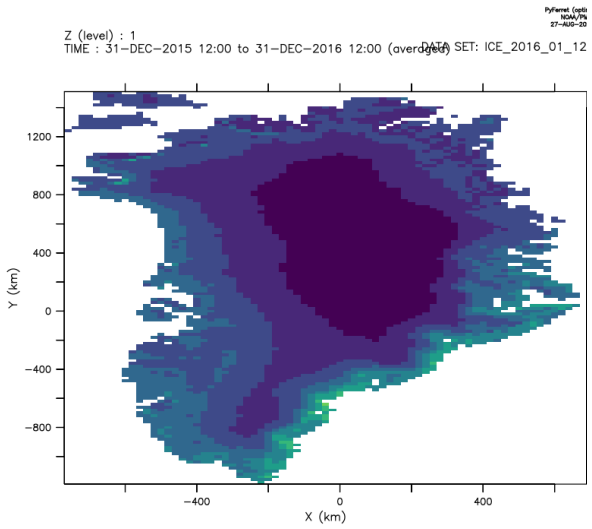

Figure 4.7: Map for Linear scheme

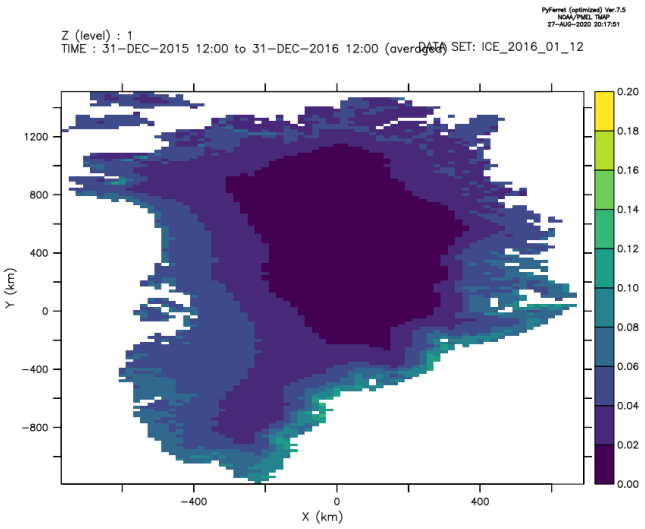

Figure 4.8: Map for Linear-bands scheme

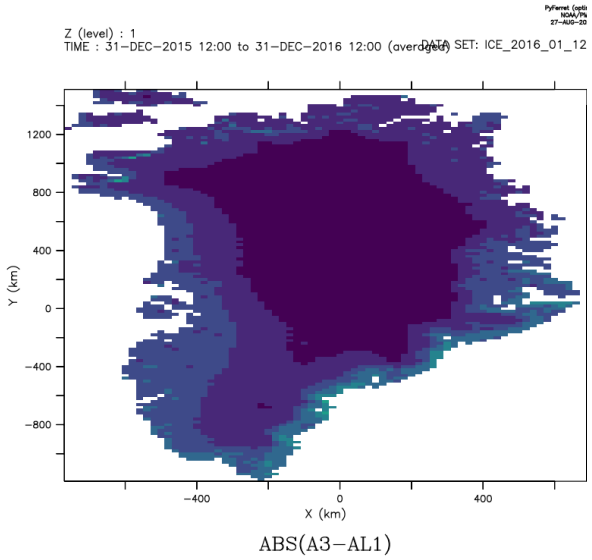

Figure 4.9: Map for Polynomial scheme

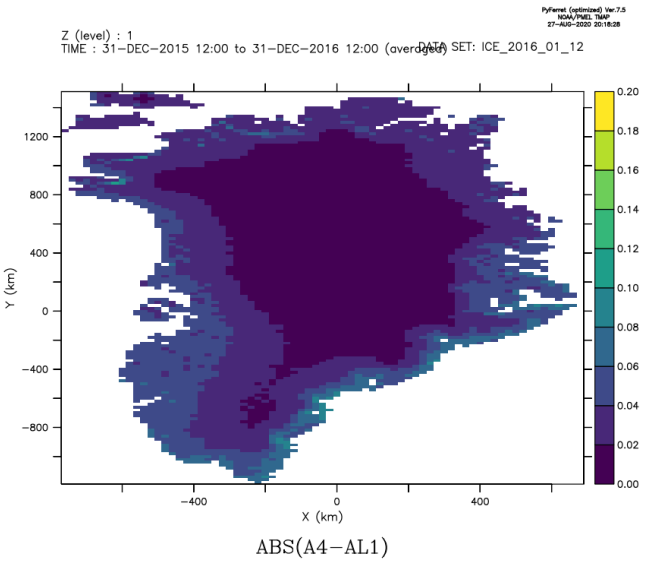

Figure 4.10: Map for Polynomial-bands scheme

Chapter 5

Conclusions

From the literature discussion, results obtained, and mapping, it is concluded that the polynomial scheme is the better approach. However, this is a large RMSE for albedo which suggests that a more complex scheme is needed; one that at minimum accounts for snow fall and snow depth as discussed in Section 2.

It was not possible to determine weather the band-schemes have a greater accuracy than the broadband schemes or not, as the error differences between band-schemes and broadband-schemes are small, and the parameterization only models the broadband albedo of snow; however, the chosen sites from which data was retrieved, do present other types of surfaces, such as: ice surfaces, snowfalls, and impurities (dust, algae, and carbon particles). Particularly for the MAR simulated data set, the RMSE's are large and relatively unexpected, as the polynomial schemes (which had performed best) performed the worst. However, it is not surprising given all the uncertainties, especially given that this data set is provides simulated albedo, and not real observations.

Each scheme makes its own approximations and assumptions in order to model albedo. Therefore, the best option is to choose the simplest model, unless there is

a clear physical reason to choose another model. Which, as previously highlighted in the literature review, and in the results section, the best scheme would be the polynomial-bands scheme as it showed to have lower MAE errors than the linear schemes, lower spatial errors (mapped Absolute Error), and it takes into account some of the key variables highlighted in the literature review: wavelength, temperature, and time (accounting for the non-instantaneous albedo transformations when temperature increases causing melt).

For future direction, any scheme should take into account the key aspects discussed in the literature review in order to properly simulate the albedo evolution for snow; thus, a complex model that accounts for: wavelength, temperature, time, and especially snow depth which allows us to distinguish between surfaces. It is also highlighted that future scheme comparisons should evaluate the efficiency of the constants and ranges, as these parameters do affect the model's performance and are usually not compared.

References

Baptist, V. (2018). Surface energy balance and modelled firn density, Greenland ice sheet, 1998-2015. Arctic Data Center. doi: 10.18739/A2D795B1R

Chai, T., Draxler, R. (2014). Root mean square error (RMSE) or mean absolute error (MAE) - Arguments against avoiding RMSE in the literature, Geoscientific Model Development, 7(3), 1247-1250. doi: 10.5194/gmd-7-1247-2014

Coakley, J. (2003). Reflectance and albedo, surface. Encyclopedia of Atmospheric Sciences. doi: 10.1016/B0-12-227090-8/00069-5

Collins, W. (2002), Description of the NCAR Community Atmosphere model (CAM2). http://www.ccsm.ucar.edu/models/atm-cam/docs/description/index.html

Dang, C., Q. Fu, Warren, S.G. (2016). Effect of Snow Grain Shape on Snow Albedo. J. Atmos. Sci., 73, 3573-3583, doi: 10.1175/JAS-D-15-0276.1

Fettweis, X., Rennermalm, A. (2020). Model simulations from Modele Atmospherique Regionale (MAR) over Greenland, 1948-2016. Arctic Data Center. doi: 10.18739/A2H12V80V

Gardner, A. S., Sharp, M. J. (2010). A review of snow and ice albedo and the

development of a new physically based broadband albedo parameterization, J. Geophys. Res., 115, F01009, doi: 10.1029/2009JF001444.

Geophysical Fluid Dynamics Laboratory. (no date). Climate Modeling. Retrieved August 1, 2020, from https://www.gfdl.noaa.gov/climate-modeling/

IPCC (2019). IPCC Special Report on the Ocean and Cryosphere in a Changing Climate [H.-O. Portner, D.C. Roberts, V. Masson-Delmotte, P. Zhai, M. Tignor, E. Poloczanska, K. Mintenbeck, A. Alegria, M. Nicolai, A. Okem, J. Petzold, B. Rama, N.M. Weyer (eds.)]. In press.

Oerlemans, J., Knap, W.H. (1998). A 1 Year Record of Global Radiation and Albedo in the Ablation Zone of Morteratschgletscher, Switzerland. Journal of Glaciology. 44. doi: 10.1017/S0022143000002574.

Oerlemans, J. (2010). The microclimate of valley glaciers. Utrecht, Utrecht University. Igitur, Utrecht Publishing and Archiving Services. 138pp. ISBN 987-9-039-35305-5, paperback. Available free from j.oerlemans@uu.nl and as free download from http://igitur-archive.library.uu.ni

Klok, E.J., Oerlemans, J. (2004). Climate Reconstructions Derived from Global Glacier Length Records, Arctic, Antarctic, and Alpine Research, 36:4, 575-583, doi: 10.1657/1523-0430(2004)036[0575:CRDFGG]2.0.CO;2

Koltzow, M. (2007), The effect of a new snow and sea ice albedo scheme on regional climate model simulations,J. Geophys. Res., 112, D07110, doi: 10.1029/2006JD007693

NASA, Lindsey, R. (2009). Climate and Earth's Energy Budget. Retrieved August 1, 2020, from https://earthobservatory.nasa.gov/features/EnergyBalance

NASA, Thekaekara, M. P. (1976). Solar irradiance: total and spectral and its possible variations. Applied Optics, 15(4), 915. doi:10.1364/ao.15.000915

NOAA. (no date). Climate Models | NOAA Climate.gov. Climate. Retrieved August 1, 2020, from https://www.climate.gov/maps-data/primer/climate-models

Qunzhu, Z., Meisheng, C., Feng, X., Fengxian, L., Xianzhang, C., Wenkun, S. (1984). A study of spectral reflection characteristics for snow, ice and water in the north of China. Hydrological Applications of Remote Sensing and Remote Data Transmission. 145.

Roesch, A. (1999). Assessment of the land surface scheme in climate models with focus on surface albedo and snow cover. (Doctoral dissertation, ETH Zurich).

Roesch, A., Gilgen, H., Wild, M., Ohmura, A. (1999). Assessment of GCM simulated snow albedo using direct observations. Climate Dynamics. 15. 405-418. doi: 10.1007/s003820050290.

Roesch, A. (2002). Comparison of spectral surface albedos and their impact on the general circulation model simulated surface climate. Journal of Geophysical Research, 107(D14). doi: 10.1029/2001jd000809

Warren, S. G., R. E. Brandt, T. C. Grenfell, and C. P. McKay (2002), Snowball Earth: Ice thickness on the tropical ocean, J. Geophys. Res., 107(C10), 3167, doi: 10.1029/2001JC001123.

Willmott, C., Matsuura, K. (2005). Advantages of the Mean Absolute Error (MAE) over the Root Mean Square Error (RMSE) in Assessing Average Model Performance. Climate Research. 30. 79. doi: 10.3354/cr030079.

Wiscombe, W., Warren, S. (1980). A Model for the Spectral Albedo of Snow. I: Pure Snow. Journal of The Atmospheric Sciences - J ATMOS SCI. 37. 2712-2733. doi: 10.1175/1520-0469(1980)037<2712:AMFTSA>2.0.CO;2.

Appendix

A.1 Code Description

The following C code, models and validates the selected snow albedo schemes for Dye2 and Crawford Point surfaces. It considers two variables per data set: measured albedo (A) and surface temperature (ST); both variables are documented in the NetCDF files, and have the same number of points.

Surface temperature had all of its points associated with a particular value; however, the variable 'measured albedo' was incomplete as several points had not been assigned a value. When the data was exported from a NetCDF to an ASCII file, all of the points associated with a NaN value were not included, making the resulting file have less points than its original. As such, it was necessary to account for this lack of points in the code. This was done by exporting the variable along with its associated point, so that it was possible to locate which points specifically were actually being used. The resulting files had a column for the variable (A or ST) and another for the actual data point that was associated with the variable value.

The program takes this into account by first scanning the variable 'measured albedo' (the variable with missing values), then registering the measured albedo in the array $A[j]$ and the non-empty data point associated with a particular value in the array $n[j]$. Once the existing points ($n[j]$) are registered, the program then scans the

surface temperature data file at the specific point $i = n[j]$ which we know to exist as it is the point associated with the measured snow albedo value, and assigns value to the array $T[i]$.

The complete code is provided bellow.[1]

```
#include <stdio.h>
#include <math.h>
#include <time.h>
#include <string.h>
// MAX AND MIN FUNCTIONS
double max(double x, double y){
    double result;
    if (x > y){
        return x;
    }
    else return y;
}
double min(double x, double y){
    double result;
    if (x < y) {
        return x;
    }
    else return y;
}
// TEMPERATURE SCALING FACTOR
double Tscale(double T, double T0, double TM){
```

[1]Comments in C language are stablished with a double dash: //

```
    double result;
    result = min(1,max(0,(T - T0)/(TM-T0)));
    return result;
}
// ALBEDO SCHEMES
double Linear(double tscale, double MAX, double MIN){
    double result;
    result = MAX - (MAX - MIN)*tscale;
    return result;
}
double Poly(double T, double MAX, double MIN){
    double result;
    result = min(MAX,max(MIN,MIN + (-0.0758627)*pow(T,1) +
        (-5.5360168E-3)*pow(T,2) + (-5.2966269E-5)*pow(T,3) +
        (4.2372742E-6)*pow(T,4)));
    if (T < -10){ result = MAX; }
    if (T > 0){ result = MIN;}
    return result;
}
double PolyVIS(double T,double temp, double MAX, double MIN){
    double result;
    result = min(MAX,max(MIN,0.57 + (-0.0758627)*pow(T,1) +
        (-5.5360168E-3)*pow(T,2) + (-5.2966269E-5)*pow(T,3) +
        (4.2372742E-6)*pow(T,4)));

    if (temp <= 268.9){ result = 0.8; }
```

```
    if (result == 0.8 ){result = MAX - (MAX - 0.8)*min(1,max
        (0,(temp - 263.15)/(268.9-263.15)));}
    return result;
}
//BROADBAND CONVERSION SCHEMES
double KnapConv(double VIS,double NIR){
    double result;
    result = 0.53*VIS + 0.47*NIR;
    if (result > 0.8){result = 0.8;}
    if (result < 0.5){result = 0.5;}
    return result;
}

// MAIN CODE
int main(){
    FILE *TS;
    FILE *ALBEDO;
    FILE *Results_tscale;
    FILE *Results_linear;
    FILE *Results_linBANDS;
    FILE *Results_poly;
    FILE *Results_polyBANDS;
    FILE *Results_MAE;
    FILE *Results_RMSE;
//Input Files
    TS = fopen("TS_C.dat","r");
```

```
    ALBEDO = fopen("AlbedoC.dat","r");
//Output Files
    Results_tscale = fopen("Tscale.dat","w");
    Results_linear = fopen("Linear.dat","w");
    Results_poly = fopen("Poly.dat","w");
    Results_polyBANDS = fopen("PolyBANDS.dat","w");
    Results_linBANDS = fopen("LinBANDS.dat","w");
    Results_MAE = fopen("MAE.dat","w");
    Results_RMSE = fopen("RMSE.dat","w");
//Parametrization
    int i=0,j=0,k=0;
    double temp,tscale;
    int points = 114889; //Adjust to match data set
    double Lin[points],LinVIS,LinNIR,LinBANDS[points];
    double poly[points],polyVIS,polyNIR,polyBANDS[points];
    double SumMAE[4] = {0,0,0,0}; //for schemes: linear, lin-
       bands, polynomial, poly-bands
    double SumRMSE[4] = {0,0,0,0};
    double T[points],A[points];
    int n[points];

    while (j < points){
        fscanf(ALBEDO,"%d %lf\n",&n[j],&A[j]);
        i = n[j];
        fscanf(TS,"%*d %lf\n",&T[i]);
        tscale = Tscale(T[i],263.15,273.15);
```

```
//Linear schemes
        Lin[j] = Linear(tscale,0.8,0.5);
        LinVIS = Linear(tscale,0.95,0.57);
        LinNIR = Linear(tscale,0.65,0.39);
        LinBANDS[j] = KnapConv(LinVIS,LinNIR);
//Polynomial Schemes
        poly[j] = Poly(T[i]-273.15,0.8,0.5);
        polyVIS = PolyVIS(T[i]-273.15,T[i],0.95,0.57);
        polyNIR = Poly(T[i]-273.15,0.65,0.39);
        polyBANDS[j] = KnapConv(polyVIS,polyNIR);
//MAE summation
        SumMAE[0] = SumMAE[0] + fabs(Lin[j]-A[j]); //linear
        SumMAE[1] = SumMAE[1] + fabs(LinBANDS[j]-A[j]);
        SumMAE[2] = SumMAE[2] + fabs(poly[j]-A[j]);
        SumMAE[3] = SumMAE[3] + fabs(polyBANDS[j]-A[j]);
//RMSE summation
        SumRMSE[0] = SumRMSE[0] + pow((Lin[j]-A[j]),2);
        SumRMSE[1] = SumRMSE[1] + pow((LinBANDS[j]-A[j]),2);
        SumRMSE[2] = SumRMSE[2] + pow((poly[j]-A[j]),2);
        SumRMSE[3] = SumRMSE[3] + pow((polyBANDS[j]-A[j]),2);
//Printing Scheme Results
        fprintf(Results_tscale,"\%d␣\%lf\n",i,tscale);
        fprintf(Results_linear,"\%d␣\%lf␣\%lf\n",i,T[i],Lin[j
            ]);
        fprintf(Results_linBANDS,"\%d␣\%lf␣\%lf\n",i,T[i],
            LinBANDS[j]);
```

```
            fprintf(Results_poly,"%d %lf %lf\n",i,T[i],poly[j]);
            fprintf(Results_polyBANDS,"%d %lf %lf\n",i,T[i],
                polyBANDS[j]);

            j++;
//Printing Mean Absolute Errors and Root Mean Squared Errors
            if (j== points){
                for (k=0;k<4;k++){
                    fprintf(Results_MAE,"\%d \%lf\n",k+1,(SumMAE[
                        k])/points);
                    fprintf(Results_RMSE,"\%d \%lf\n",k+1,sqrt((
                        SumRMSE[k])/points));
                    }
            }
        }
        return 1;
}
```

A.2 FERRET Algorithms

Here are listed the given commands within the terminal, in order to get the FERRET software to model snow albedo, as well as mapping the MAErros.

The MAE and RMSE were calculate through the use of the command *stats* < *Variablename* > which calculates the mean value for the specified variable. Particularly, the command *stats*MAE calculates the mean value for the absolute error (the mean absolute error) and *stats*RMSE calculates the Mean Squared Error

($\frac{\Sigma(predicted-actual)^2}{n}$); thus, the squared root of the mean squared values was taken in order to obtain the RMSE.

The algorithms are provided below. [1]

```
!PARAMETRIZATION
!Linear
let A1 = .8 -(0.8 - 0.5)*min(1,max(0,(ST+10)/10))
!LinearBANDS
let Avis = .95 -(0.95- 0.57)*min(1,max(0,(ST+10)/10))
let Anir = .65 -(0.65 - 0.39)*min(1,max(0,(ST+10)/10))
let Avis = .95 -(0.95- 0.57)*min(1,max(0,(ST+10)/10))
let A2 = min(0.8,max(0.5,0.57*Avis + 0.47*Anir))
!Polynomial
let poly = min(0.8,max(0.5, 0.5 + (-0.0758627)*ST +
   (-5.5360168E-3)*ST^2 + (-5.2966269E-5)*ST^3 + (4.2372742E
   -6)*ST^4))
let A3 = IF ST LT -10 THEN 0.8 ELSE poly
!PolynomialBANDS
let polyVIS = min(0.8,max(0.57, 0.57 + (-0.0758627)*ST +
   (-5.5360168E-3)*ST^2 + (-5.2966269E-5)*ST^3 + (4.2372742E
   -6)*ST^4))
let ApfVIS = IF ST LT -4.25 THEN 0.95 - (0.95-0.8)*min(1,max
   (0,(ST+10)/(-4.25+10))) ELSE polyVIS
let polyNIR = min(0.65,max(0.39,0.39 + (-0.0758627)*ST +
   (-5.5360168E-3)*ST^2 + (-5.2966269E-5)*ST^3 + (4.2372742E
   -6)*ST^4))
```

[1] Comments in FERRET are stablished with an exclamation symbol: !

```
let ApfNIR = IF T LT -10 THEN 0.65 ELSE polyNIR
let A4 = min(0.8,max(0.5,(0.57*ApfVIS + 0.47*ApfNIR)))
!Mean Absolute Error
let MAE1 = ABS(A1-AL1)
let MAE2 = ABS(A2-AL1)
let MAE3 = ABS(A3-AL1)
let MAE4 = ABS(A4-AL1)
!Root Mean Squared Error
let RMSE1 = (A1-AL1)^2
let RMSE2 = (A2-AL1)^2
let RMSE3 = (A3-AL1)^2
let RMSE4 = (A4-AL1)^2
```

A.2.1 Mapping the Absolute Error

The shading of each grid cell was carried out with the following commands. Note that L (the time axis name in ferret) and the Z axis were set to constants, average time and 1 respectively, in order to reduce the grid dimensions, allowing FERRET to shade it. Note that the the variables named "MAE "declared in ferret are in reality the absolute error.

```
shade/lev=(0,0.2,0.02) MAE1[L=@ave,Z=1]
shade/lev=(0,0.2,0.02) MAE2[L=@ave,Z=1]
shade/lev=(0,0.2,0.02) MAE3[L=@ave,Z=1]
shade/lev=(0,0.2,0.02) MAE4[L=@ave,Z=1]
```